

# Multifunctional, Defect-Engineered Metal–Organic Frameworks with Ruthenium Centers: Sorption and Catalytic Properties\*\*

Olesia Kozachuk, Ignacio Luz, Francesc X. Llabrés i Xamena, Heshmat Noei, Max Kauer, H. Bauke Albada, Eric D. Bloch, Bernd Marler, Yuemin Wang,\* Martin Muhler, and Roland A. Fischer\*

**Abstract:** A mixed-linker solid-solution approach was employed to modify the metal sites and introduce structural defects into the mixed-valence Ru<sup>II/III</sup> structural analogue of the well-known MOF family [M<sub>3</sub><sup>II/III</sup>(btc)<sub>2</sub>] (M = Cu, Mo, Cr, Ni, Zn; btc = benzene-1,3,5-tricarboxylate), with partly missing carboxylate ligators at the Ru<sub>2</sub> paddle-wheels. Incorporation of pyridine-3,5-dicarboxylate (pydc), which is the same size as btc but carries lower charge, as a second, defective linker has led to the mixed-linker isorecticular derivatives of Ru-MOF, which display characteristics unlike those of the defect-free framework. Along with the creation of additional coordinatively unsaturated sites, the incorporation of pydc induces the partial reduction of ruthenium. Accordingly, the modified Ru sites are responsible for the activity of the “defective” variants in the dissociative chemisorption of CO<sub>2</sub>, the enhanced performance in CO sorption, the formation of hydride species, and the catalytic hydrogenation of olefins.

The great diversity and modularity of metal–organic frameworks (MOFs) suggest that they may compete with traditional porous materials for many applications.<sup>[1]</sup> Many processes at MOFs involve interactions between metal sites and guest molecules. Thus, the generation and control of reactive, coordinatively unsaturated sites (CUS) within the molecular scaffolds is highly desirable.<sup>[2]</sup> Generally, MOFs result from the self-assembly of inorganic and organic building blocks to form porous and highly ordered crystalline solids: all metal ions are kept by the linkers at fixed positions in a lattice in,

ideally, exactly the same coordination environment. CUS are commonly generated when solvent molecules ligating metal centers are removed during activation, for instance, at the axial positions of paddle-wheel units in [M<sub>3</sub><sup>II/III</sup>(btc)<sub>2</sub>] (M = Cu,<sup>[3]</sup> Mo,<sup>[4]</sup> Cr,<sup>[5]</sup> Ni,<sup>[6]</sup> or Zn;<sup>[7]</sup> btc = benzene-1,3,5-tricarboxylate). Meanwhile, a particular challenge is to enhance the accessibility, even lower the coordination number, and thus modify the local structure and proximate space with respect to the intrinsic metal ion framework sites by the introduction of so-called “structural point defects” originating from partly or even completely missing linker(s) and connections between the metal nodes. The introduction of such defects should, however, not compromise the overall integrity and robustness of the framework.<sup>[8]</sup> The modified CUS are likely to behave differently from the parent CUS and are expected to offer novel opportunities for modulating the catalytic activity and sorption behavior of MOFs. The presence of defects in the MOF can have significant effects on the catalytic properties of the material. These defects can come simply from an imperfect crystallization of the MOF,<sup>[9]</sup> or be created in a controlled manner by the introduction of auxiliary ligands with missing carboxylate group(s).<sup>[10,11]</sup>

Here, we report on a series of defect-engineered variants **D1–D4** (Figure 1) derived by framework incorporation of defect-generating linkers into the parent Ru<sup>II/III</sup> mixed-valence compound [Ru<sub>3</sub>(btc)<sub>2</sub>Cl<sub>1.5</sub>] (**1**).<sup>[12]</sup> We demonstrate that multifunctional properties of **D1–D4** are enhanced or even absent with respect to **1**, and ranging from quite unusual

[\*] O. Kozachuk, Prof. Dr. R. A. Fischer  
Chair of Inorganic Chemistry II, Ruhr-University Bochum  
Universitätsstrasse 150, 44801 Bochum (Germany)  
E-mail: roland.fischer@ruhr-uni-bochum.de

I. Luz, Dr. F. X. Llabrés i Xamena  
Instituto de Tecnología Química (ITQ)  
Universidad Politécnica de Valencia  
Consejo Superior de Investigaciones Científicas  
Avenida de los Naranjos s/n, 46022 Valencia (Spain)

Dr. H. Noei, Dr. Y. Wang, Prof. Dr. M. Muhler  
Laboratory of Industrial Chemistry  
Ruhr-University Bochum (Germany)


M. Kauer, Dr. Y. Wang  
Chair of Physical Chemistry I, Ruhr-University Bochum  
Universitätsstrasse 150, 44801 Bochum (Germany)  
E-mail: wang@pc.rub.de

Dr. H. B. Albada  
Chair of Inorganic Chemistry I—Bioinorganic Chemistry  
Ruhr-University Bochum (Germany)

E. D. Bloch  
Department of Chemistry  
University of California, Berkeley (USA)

Dr. B. Marler  
Faculty of Geosciences  
Institute of Geology, Mineralogy and Geophysics  
Ruhr-University Bochum (Germany)

[\*\*] O.K. acknowledges Ruhr-University Research School (<http://www.research-school.rub.de>) for admission and additional support of her PhD project. I.L. and F.X.L.X. acknowledge support by Consolider-Ingenio 2010 (project MULTICAT) and the “Severo Ochoa” program.

 Supporting information for this article (synthesis of **D1–D4** as well as details of the analytical and characterization methods, full PXRD, FTIR, TG, SEM, BET, far-IR, XPS, UHV-FTIR, HPLC, <sup>1</sup>H NMR analysis, elemental analysis (Ru, C, H, N, Cl), and sorption and catalytic data) is available on the WWW under <http://dx.doi.org/10.1002/anie.201311128>.

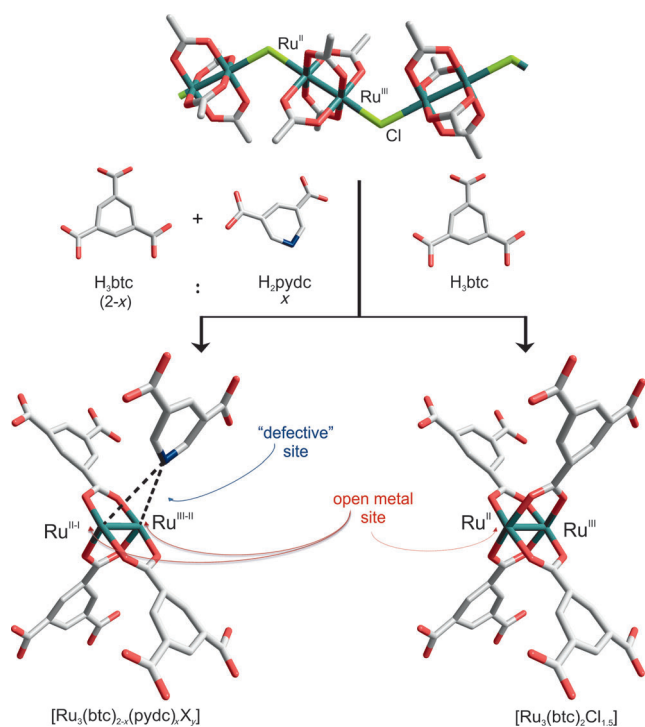


**Figure 1.** Defect-engineered  $[\text{Ru}_3(\text{btc})_{2-x}(\text{pydc})_x\text{X}_y]$  ( $\text{X} = \text{Cl}, \text{OH}, \text{OAc}$ ;  $x = 0.1$  (**D1**),  $0.2$  (**D2**),  $0.6$  (**D3**),  $1$  (**D4**);  $0 \leq y \leq 1.5$  (left) and parent  $[\text{Ru}_3(\text{btc})_2\text{Cl}_{1.5}]$  (**1**) (right).

$\text{CO}_2 \rightarrow \text{CO}$  dissociative chemisorption (“reduction”) at 90 K under ultrahigh-vacuum conditions (UHV) to hydrogen splitting (Ru-H formation) at ambient conditions and related hydrogenation catalysis.

The concept of mixed-linker solid solutions<sup>[13]</sup> was applied to obtain the single-phased  $[\text{Ru}_3(\text{btc})_{2-x}(\text{pydc})_x\text{X}_y]$  (**D1–D4**) by using mixtures of  $\text{H}_2\text{btc}$  and pyridine-3,5-dicarboxylic acid ( $\text{H}_2\text{pydc}$ ) in the synthesis (Figure 1). The (deprotonated) linkers  $\text{btc}^{3-}$  and  $\text{pydc}^{2-}$  are quite similar in size and structure, but  $\text{pydc}$  has one less carboxylate ligator site. The Cu analogues  $[\text{Cu}_3(\text{btc})_{2-x}(\text{pydc})_x\text{X}_y]$  ( $\text{X} = \text{NO}_3^-$ , etc.) had been synthesized and studied previously.<sup>[8b]</sup> From inspection of the powder X-ray diffraction patterns (PXRD) of the as-synthesized and activated samples it is deduced that **D1–D4** are isostructural to the parent single-linker **1** as well as to  $[\text{Cu}_3(\text{btc})_2]$  (HKUST-1, MOF-199) and its  $\text{btc}/\text{pydc}$  mixed-linker variants. The samples exhibit permanent microporosity with surface area values similar to that of **1** (Figures S3–S6, Table S1 in the Supporting Information). While in its X-ray photoelectron spectrum (XPS) the parent **1** features spin-orbit doublet peaks ( $\text{Ru}3d_{5/2}$  and  $3d_{3/2}$  region) at 281.5 and 285.7 eV, as well as at 282.5 and 286.7 eV characteristic for the  $\text{Ru}^{\text{II}}$  and  $\text{Ru}^{\text{III}}$  species,<sup>[12]</sup> an extra doublet at about 280.3 and 284.5 eV appears for **D1–D3** (Figures S7 and S8; sample **D4** was not measured). This new doublet increases gradually in intensity and shifts to 280.0/284.2 eV when the concentration of the defective linker  $\text{pydc}$  increases, indicating the presence of additional  $\text{Ru}^{\delta+}$  species that are more electron-rich than  $\text{Ru}^{\text{II/III}}$ . The formation of reduced  $\text{Ru}^{\delta+}$  is accompanied by the attenuation of both the  $\text{Ru}^{\text{III}}3d$  peaks (at 282.5 and 286.7 eV)

and  $\text{Cl}2p$  peaks (at 198.4 and 200.0 eV).<sup>[12]</sup> Along with the C1s and O1s peaks of carboxylate species at 288.5 and 532.1 eV, respectively, the N1s peak at 400.2 eV is observed, which originates only from  $\text{pydc}$ . Importantly, on the basis of the O1s data, Ru oxide impurities are ruled out. These XPS data together with elemental analysis data (Tables S2 and S3 in the Supporting Information) and further analytical evidence (Figures S9–S12 in the Supporting Information) support the incorporation of  $\text{pydc}$  in the framework, resulting in randomly distributed reduced, mixed-valence  $\text{Ru}_2$  paddlewheel units in which  $\text{pydc}$  partly replaces the parent  $\text{btc}$  and with or without (residual) counter ion(s) or ligands at the axial Ru sites (Figure 1).

$\text{CO}$  adsorption isotherms at 298 K were recorded to investigate the effect of the  $\text{pydc}$  incorporation on the sorption capacity and showed an increased uptake. For example, activated **D3** displayed a total uptake of  $3.88 \text{ mmol g}^{-1}$ , whereas the parent **1** had a 28% lower uptake value of  $2.8 \text{ mmol g}^{-1}$  (Figure S13 and Table S4 in the Supporting Information). Hence, to gain more detailed insight, the  $\text{CO}$  adsorption was monitored in situ by UHV-FTIR spectroscopy at 90 K (Figures S14 and S15 in the Supporting Information).<sup>[14]</sup> Interestingly, two new intense bands at lower wavenumbers are seen at  $2000$  and  $2039 \text{ cm}^{-1}$  for **D1–D3**, which are absent for the parent **1**<sup>[12b]</sup> and are highly sensitive to the doping level of  $\text{pydc}$ . These pronounced red-shifted bands are characteristic for various  $\text{CO}$  species adsorbed on  $\text{Ru}^{\delta+}$  ( $0 < \delta < 2$ ) centers (Table 1). Temperature-dependent  $\text{CO}$  desorption experiments display the fast decrease of the higher-lying bands at  $2171$  and  $2118 \text{ cm}^{-1}$  upon heating. Their complete disappearance at 130 K and 190 K indicates the weak binding of  $(\text{CO})\text{Ru}^{3+}$  and the comparatively stronger binding of  $(\text{CO})\text{Ru}^{2+}$ , respectively.

**Table 1:** UHV-FTIR data for  $\text{CO}$  and  $\text{CO}_2$  adsorption at Ru species.

Sample	Band [ $\text{cm}^{-1}$ ]	Assignment
<i>CO exposure</i>		
parent Ru-MOF ( <b>1</b> )	2171, 2137	$(\text{CO})\text{Ru}^{3+}$ , $(\text{CO})\text{Ru}^{2+}$
<b>D1</b>	2174, 2133	$(\text{CO})\text{Ru}^{3+}$ , $(\text{CO})\text{Ru}^{2+}$
	<b>2045, 2002</b>	<b><math>(\text{CO})\text{Ru}^{\delta+}</math></b>
<b>D3</b>	2171, 2118	$(\text{CO})\text{Ru}^{3+}$ , $(\text{CO})\text{Ru}^{2+}$
	<b>2039, 2000</b>	<b><math>(\text{CO})\text{Ru}^{\delta+}</math></b>
<i>CO<sub>2</sub> exposure</i>		
parent Ru-MOF ( <b>1</b> )	2335, 2272	$(\text{CO}_2)\text{Ru}^{2+}$ , $(\text{CO}_2)\text{Ru}^{3+}$
<b>D1</b>	2335, 2272	$(\text{CO}_2)\text{Ru}^{2+}$ , $(\text{CO}_2)\text{Ru}^{3+}$
	<b>2039, 2000</b>	<b><math>(\text{CO})\text{Ru}^{\delta+}</math></b>
<b>D3</b>	2335, 2272	$(\text{CO}_2)\text{Ru}^{2+}$ , $(\text{CO}_2)\text{Ru}^{3+}$
	<b>2039, 2000</b>	<b><math>(\text{CO})\text{Ru}^{\delta+}</math></b>

[a] Values in bold correspond to the frequencies of  $\text{CO}$  bound to reduced  $\text{Ru}^{\delta+}$ .

All further, low-lying bands disappear only at about 280 K, supporting the assignment of these bands to  $\text{CO}$  molecules binding strongly to more electron-rich, that is, reduced  $\text{Ru}^{\delta+}$  sites due to enhanced  $\pi$ -backdonation (Figure S15 in the Supporting Information). Our related theoretical studies on  $\text{CO}$  binding to the parent **1** have shown<sup>[12b]</sup> that the local

organization of this “non-defective” framework is also not straightforward. Rather, the simultaneous existence of two different types of Ru<sup>II/III</sup> paddle-wheels, one in which two Cl<sup>-</sup> anions are coordinated at each of the two Ru sites and one in which both Ru atoms are not coordinated, provided the best match with the experiment. These reference data also make it possible to rule out the interpretation of **D1–D4** as a physical mixture of **1** with various amounts of Ru nanoparticles (NPs), because in such a case the intensity ratio of the (CO)Ru<sup>3+</sup> and (CO)Ru<sup>2+</sup> species as well as their  $\nu(\text{CO})$  frequencies would not depend on the pydc concentration applied during synthesis. Rather, **D1–D4** reveal more than two nonequivalent and accessible framework Ru sites different from that in **1** (even at low concentrations of pydc). Notably, related CO adsorption studies monitored by UHV-FTIRS on [Cu<sub>3</sub>(btc)<sub>2</sub>] thin-film (SURMOFs) materials showed about 4% of defective copper sites, which were identified as mixed-valence Cu<sup>I</sup>/Cu<sup>II</sup> paddle-wheels.<sup>[8d]</sup> Hence, owing to the gradual decrease in overall anionic charge upon increasing pydc doping, the response of the framework in the reduction of Ru sites is quite plausible.

Inspired by the above findings we expected unique properties of the defect-engineered samples in comparison to the parent **1**. First, we studied low-temperature CO<sub>2</sub> adsorption (UHV-FTIRS). Most surprisingly, after CO<sub>2</sub> adsorption on **D1–D3** two dominating, low-lying bands were observed at 2039 and 2000 cm<sup>-1</sup> which are characteristic of (CO)Ru<sup>δ+</sup> species, and this unambiguously indicates CO<sub>2</sub>→CO reduction. Importantly, for defect-free **1** only bands at 2335 and 2272 cm<sup>-1</sup> are observed, which are characteristic of weakly physisorbed CO<sub>2</sub>, coordinated in linear fashion to Ru sites. The intensity of these CO<sub>2</sub>-related bands gradually decreases with increasing pydc doping in the series **D1–D3**, while a significant enhancement of the low-lying bands assigned to (CO)Ru<sup>δ+</sup> is observed (Table 1, Figure 2). It should be noted that dissociative chemisorption of CO<sub>2</sub> in the dark was not observed for Ru NPs.<sup>[15]</sup>

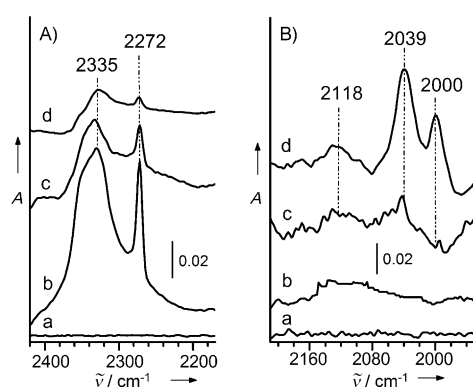
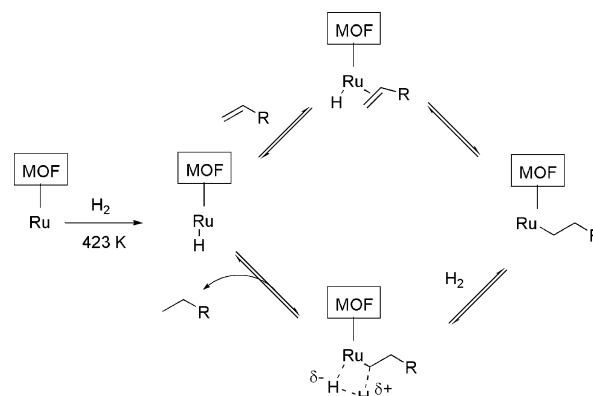


**Figure 2.** UHV-FTIR spectra (the regions of CO<sub>2</sub> (A) and CO (B) vibrations are displayed) obtained at 90 K after exposing the parent **1** (b) and defect-engineered **D1** (c) and **D3** (d) (representative samples) to CO<sub>2</sub> ( $1 \times 10^{-4}$  mbar). Traces (a) represent spectra of **1** prior to the CO<sub>2</sub> exposure. Temperature-dependent desorption experiments are given in the Figures S16 and S17 in the Supporting Information.

Photoinduced reduction of CO<sub>2</sub> to CO and other valuable organic molecules has been found on semiconducting nano-materials (e.g. TiO<sub>2</sub>, CdS, ZnO) under irradiation with UV or visible light.<sup>[16]</sup> Additionally, electrochemical reduction of CO<sub>2</sub> on various metallic electrodes has been reported.<sup>[17]</sup> For MOFs, however, such a property is rather unprecedented and very few exhibit activity towards CO<sub>2</sub> conversion.<sup>[18]</sup> Namely, for the CO<sub>2</sub>→CO photocatalytic reduction only UiO-67 functionalized with [Re<sup>I</sup>(dcby)(CO)<sub>3</sub>Cl] (dcby = 2,2'-bipyridine-5,5'-dicarboxylic acid) was reported.<sup>[18a]</sup> A number of Ru<sup>II</sup> and Ru<sup>I</sup> complexes are known to be efficient in the photo- and electrocatalytic reduction of CO<sub>2</sub> providing CO or formic acid (or formates) as the products.<sup>[19]</sup> Since the reaction on **D1–D3** also takes place in the dark, we rule out the photochemical pathway. Thus, considering that the defect-free parent sample **1** is totally inactive (Figure 2, traces (b)), the CO<sub>2</sub>→CO conversion at 90 K is likely to be driven by strong interactions with reduced Ru<sup>δ+</sup> CUS. Enhanced charge transfer from Ru 3d to the CO<sub>2</sub> 2π<sub>u</sub> antibonding orbital possibly yields chemisorbed CO<sub>2</sub><sup>δ-</sup> species that might act as a reaction intermediate to finally produce CO. The activation of CO<sub>2</sub> could be further promoted by pydc due to the basic pyridyl N sites in proximity to the reactive Ru sites (possible formation of pyridyl NO<sub>x</sub> species).<sup>[20]</sup> In any case, during the synthesis of **D1–D3** and formation of reduced Ru<sup>δ+</sup> centers, energy is stored in the system to allow the removal of one O atom from CO<sub>2</sub>. Unfortunately, we cannot comment on the fate of this oxygen atom.

Ru complexes have a strong tendency to perform a heterolytic, base-assisted activation of H<sub>2</sub>, instead of oxidative addition, to generate Ru–hydride species (Scheme 1).<sup>[21]</sup> Remarkably, **D1–D4** form such Ru–H species after H<sub>2</sub> treatment as revealed by FTIR spectroscopy, while the structural integrity is fully preserved (Scheme S1, Figures S18–S22 in the Supporting Information). In fact, after the samples had been heated under *p*(H<sub>2</sub>) new bands appear in the characteristic region of Ru–H vibrations at 1956–1975 and 2057–2076 cm<sup>-1</sup>.<sup>[22]</sup>



**Scheme 1.** Olefin hydrogenation involving base-assisted heterolytic splitting of H<sub>2</sub> over defect-engineered Ru-MOFs. Note that the pydc linker in **D1–D4** (Figure 1) offers a basic pyridyl-N atom in the proximity of the reactive Ru centers.

This observation prompted us to screen the catalytic properties of the samples and the influence of the defects on the catalytic performance with and without hydrogen pretreatment. Indeed, there is huge variety of reactions, well-known to be catalyzed by Ru: both homogeneous and heterogeneous (like Ru/C or RuO<sub>2</sub>, etc.).<sup>[23]</sup> Nevertheless, only few studies were reported on porous solids bearing Ru at the framework nodes and, to the best of our knowledge, none of them on Ru-CUS.<sup>[24]</sup> In view of the observed tendency of our samples to form Ru-H species, we first investigated their performance as olefin hydrogenation catalysts, using 1-octene as the model compound. To track the influence of the introduced defects, the samples **D1** with low and **D3** with high pydc doping were selected. As can be seen in Figure 3, the parent sample **1** displays only marginal hydrogenation activity, producing only 12% conversion of 1-octene after 20 h. Introduction of pydc defects led to a clear increase in

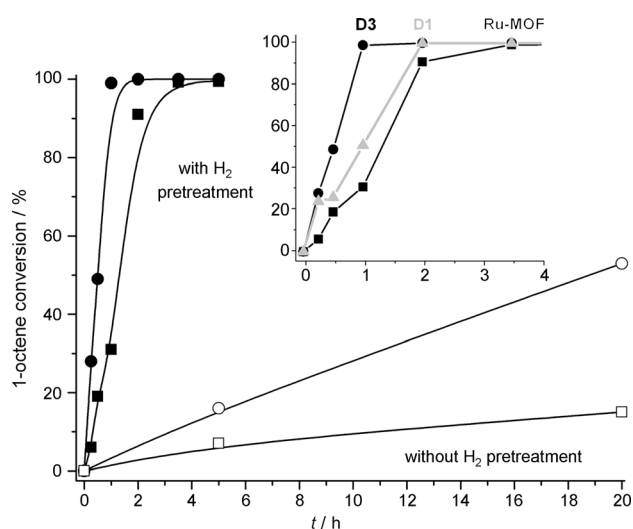


**Figure 3.** Comparison of the 1-octene conversion over various pre-treated samples (see text) represented as open symbols (without H<sub>2</sub> pretreatment) and closed symbols (with H<sub>2</sub> pretreatment): parent Ru-MOF (**1**) (□ and ■, respectively), and the defect-engineered variants **D3** (○ and ●, respectively). Insert: Comparison of the 1-octene conversion over H<sub>2</sub>-pretreated parent **1** with the samples **D1** (▲) and **D3** with different pydc contents.

activity, and the conversion of 1-octene over sample **D3** (ca. 30 mol% of pydc) was 50% after the same reaction time. Meanwhile, along with the expected product, octane, a mixture of intermediate products arising from isomerization side reactions also formed, (*E,Z*)-2-octene, (*E,Z*)-3-octene, and (*E,Z*)-4-octene, accounting for roughly 30% of the 1-octene converted (Scheme S2 and Figure S26 in the Supporting Information). This result reveals that some Ru-CUS present in the samples have a certain  $\pi$ -acid character, in good agreement with the observed behavior of parent sample **1** upon CO adsorption at 90 K, as monitored by UHV-FTIR spectroscopy (Figure S14 in the Supporting Information).

As expected, the defect-engineered samples produced slightly higher amounts of isomerization products than **1**, in

line with the increased  $\pi$ -binding properties of the defect-engineered materials. Interestingly, when the samples were pretreated in situ at  $p(\text{H}_2) = 8$  atm and 423 K for 2 h before the olefin was added at the reaction temperature, the catalytic performance for olefin hydrogenation dramatically increased (Figure 3), while olefin isomerization side reactions decreased significantly.

FTIR spectroscopy showed that the enhanced activity and selectivity for olefin hydrogenation versus the competing isomerization side reaction is due to the efficient formation of Ru-H species during pretreatment. Formation of Ru-H is most likely the rate-determining step in a process such as that depicted in Scheme 1. Notably, pydc could possibly assist this heterolytic activation by acting as a suitable base ligand (pyridyl-N site) in proximity to the reactive Ru sites. Indeed, the rate of 1-octene hydrogenation increased with the concentration of pydc, reflecting the extent of hydride species formed during the pretreatment in each sample. Thus, the time needed to attain full conversion of 1-octene was 3–4 h for the parent **1**, 2 h for **D1**, and less than 1 h for **D3** (Figure 3, insert). In all cases octane was the only product observed at the end of the reaction. Similar hydrogenation results and mechanistic interpretation were reported for Rh<sup>II</sup> carboxylate paddle-wheel MOFs.<sup>[25]</sup>

Similar to their activity in the hydrogenation of 1-octene, **D1–D3** display enhanced performance towards adsorption and interaction with shorter unsaturated hydrocarbons (e.g. ethylene; Figure S27 in the Supporting Information). They served as catalysts with a progressive trend upon increasing amount of pydc, for example in hydrogen-transfer reactions, such as the Meerwein-Ponndorf-Verley reduction of carbonyl compounds and the isomerization of allylic alcohols to saturated ketones. A more detailed evaluation of the catalytic properties as a function of doping with defective linkers (DLs) is underway and will be reported elsewhere. Let us just mention here that the modified Ru-CUS of these materials show multifunctional properties ranging from hydrogenation to oxidation and Lewis acid catalysis.

In summary, we have demonstrated the controlled introduction and the characterization of “defect” sites into an isorecticular Ru analogue of HKUST-1. Incorporation of pydc leads to partial reduction of the Ru sites at the defective paddle-wheel moieties and triggers novel reactivity, which is absent for the parent [Ru<sub>3</sub>(btc)<sub>2</sub>Cl<sub>1.5</sub>] (**1**). Thus, we anticipate that other [M<sub>3</sub>(btc)<sub>2</sub>] compounds can be similarly modified. The defective linkers (DLs) may be chosen with some variation (Figures S28–S31) and pydc may be regarded as just one representative example. Notably, the electronic modification of CUS (i.e. more electron-rich sites) is accompanied by lowered coordination number, that is, with expanded and functionalized coordination space in the proximity of the modified metal site. This combination of parameters which can be controlled by the choice of DLs (even mixtures of such DLs; Figure S31 in the Supporting Information) and framework incorporation level is likely to yield libraries of a novel kind of multivariant MOFs suitable for automated screening and property optimization.

Received: December 21, 2013

Published online: ■■■ ■■■, ■■■■■■

**Keywords:** CO<sub>2</sub> reduction · heterogeneous catalysis · hydrogen splitting · metal–organic frameworks · structural defects

- [1] a) H. Furukawa, K. E. Cordova, M. O’Keeffe, O. M. Yaghi, *Science* **2013**, *341*, 974–998; special issues: b) *Chem. Soc. Rev.* **2009**, *38*, 1213–1477; c) *Chem. Soc. Rev.* **2011**, *40*, 453–1152; d) *Chem. Rev.* **2012**, *112*, 673–1268.
- [2] a) A. Corma, H. García, F. X. Llabrés i Xamena, *Chem. Rev.* **2010**, *110*, 4606–4655; b) T. Uemura, N. Uchida, M. Higuchi, S. Kitagawa, *Macromolecules* **2011**, *44*, 2693–2697; c) Y.-Y. Fu, C.-X. Yang, X.-P. Yan, *Langmuir* **2012**, *28*, 6794–6802.
- [3] S. S. Y. Chui, S. M. F. Lo, J. P. H. Charmant, A. G. Orpen, I. D. Williams, *Science* **1999**, *283*, 1148–1150.
- [4] M. Kramer, U. Schwarz, S. Kaskel, *J. Mater. Chem.* **2006**, *16*, 2245–2248.
- [5] L. J. Murray, M. Dinca, J. Yano, S. Chavan, S. Bordiga, C. M. Brown, J. R. Long, *J. Am. Chem. Soc.* **2010**, *132*, 7856–7857.
- [6] P. Maniam, N. Stock, *Inorg. Chem.* **2011**, *50*, 5085–5097.
- [7] J. I. Feldblyum, M. Liu, D. W. Gidley, A. J. Matzger, *J. Am. Chem. Soc.* **2011**, *133*, 18257–18263.
- [8] a) L. Huang, H. Wang, J. Chen, Z. Wang, J. Sun, D. Zhao, Y. Yan, *Microporous Mesoporous Mater.* **2003**, *58*, 105–114; b) S. Marx, W. Kleist, A. Baiker, *J. Catal.* **2011**, *281*, 76–87; c) T.-H. Park, A. J. Hickman, K. Koh, S. Martin, A. G. Wong-Foy, M. S. Sanford, A. J. Matzger, *J. Am. Chem. Soc.* **2011**, *133*, 20138–20141; d) P. St. Petkov, G. N. Vayssilov, J. Liu, O. Shekhah, Y. Wang, C. Wöll, T. Heine, *ChemPhysChem* **2012**, *13*, 2025–2029.
- [9] a) C. Chizallet, S. Lazare, D. Bazer-Bachi, F. Bonnier, V. Lecoq, E. Soyer, A. Quoineaud, N. Bats, *J. Am. Chem. Soc.* **2010**, *132*, 12365–12377; b) F. X. Llabrés i Xamena, F. G. Cirujano, A. Corma, *Microporous Mesoporous Mater.* **2012**, *157*, 112–117.
- [10] U. Ravon, M. Savonnet, S. Aguado, M. E. Domine, E. Janneau, D. Farrusseng, *Microporous Mesoporous Mater.* **2010**, *129*, 319–329.
- [11] F. Vermoortele, B. Bueken, G. Le Bars, B. Van de Voorde, M. Vandichel, K. Houthoofd, A. Vimont, M. Daturi, M. Waroquier, V. Van Speybroeck, C. Kirschhock, D. E. De Vos, *J. Am. Chem. Soc.* **2013**, *135*, 11465–11468.
- [12] a) O. Kozachuk, K. Yusenko, H. Noei, Y. Wang, S. Walleck, T. Glaser, R. A. Fischer, *Chem. Commun.* **2011**, *47*, 8509–8511; b) H. Noei, O. Kozachuk, S. Amirjalayer, S. Burekaew, M. Kauer, R. Schmid, B. Marler, M. Muhler, R. A. Fischer, Y. Wang, *J. Phys. Chem. C* **2013**, *117*, 5658–5666.
- [13] A. D. Burrows, *CrystEngComm* **2011**, *13*, 3623–3642.
- [14] Y. Wang, A. Glenz, M. Muhler, C. Wöll, *Rev. Sci. Instrum.* **2009**, *80*, 113108.
- [15] J. Raskó, *Catal. Lett.* **1998**, *56*, 11–15.
- [16] a) P. Usubharatana, D. McMartin, A. Veawab, P. Tontiwachwuthikul, *Ind. Eng. Chem. Res.* **2006**, *45*, 2558–2568; b) V. P. Indrakanti, J. D. Kubicki, H. H. Schobert, *Energy Environ. Sci.* **2009**, *2*, 745–758; c) K. Mori, H. Yamashita, M. Anpo, *RSC Adv.* **2012**, *2*, 3165–3172.
- [17] a) B. Kumar, M. Llorente, J. Froehlich, T. Dang, A. Sathrum, C. P. Kubiak, *Annu. Rev. Phys. Chem.* **2012**, *63*, 541–569; b) E. E. Benson, C. P. Kubiak, A. J. Sathrum, J. M. Smieja, *Chem. Soc. Rev.* **2009**, *38*, 89–99.
- [18] a) C. Wang, Z. Xie, K. E. de Krafft, W. Lin, *J. Am. Chem. Soc.* **2011**, *133*, 13445–13454; b) Y. Fu, D. Sun, Y. Chen, R. Huang, Z. Ding, X. Fu, Z. Li, *Angew. Chem.* **2012**, *124*, 3420–3423; *Angew. Chem. Int. Ed.* **2012**, *51*, 3364–3367.
- [19] a) Y. Tsukahara, T. Wada, K. Tanaka, *Chem. Lett.* **2010**, *39*, 1134–1135; b) Z. Chen, C. Chen, D. R. Weinberg, P. Kang, J. J. Concepcion, D. P. Harrison, M. S. Brookhart, T. J. Meyer, *Chem. Commun.* **2011**, *47*, 12607–12609; c) N. Planas, T. Ono, L. Vaquer, P. Miró, J. Benet-Buchholz, L. Gagliardi, C. J. Cramer, A. Llobet, *Phys. Chem. Chem. Phys.* **2011**, *13*, 19480–19484.
- [20] S. L. Jain, B. Sain, *Chem. Commun.* **2002**, 1040–1041.
- [21] a) H. D. Kaesz, R. B. Saillant, *Chem. Rev.* **1972**, *72*, 231–281; b) D. Sellmann, R. Prakash, F. W. Heinemann, M. Moll, M. Klimowicz, *Angew. Chem.* **2004**, *116*, 1913–1916; *Angew. Chem. Int. Ed.* **2004**, *43*, 1877–1880.
- [22] a) X. Wang, L. Andrews, *J. Phys. Chem. A* **2009**, *113*, 551–563; b) C. P. Laua, S. M. Nga, G. Jia, Z. Lin, *Coord. Chem. Rev.* **2007**, *251*, 2223–2237.
- [23] a) K. Yamaguchi, N. Mizuno, *Angew. Chem.* **2003**, *115*, 1518–1521; *Angew. Chem. Int. Ed.* **2003**, *42*, 1480–1483; b) F. Su, F. Y. Lee, L. Lv, J. Liu, X. N. Tian, X. S. Zhao, *Adv. Funct. Mater.* **2007**, *17*, 1926–1931; c) H. Over, *Chem. Rev.* **2012**, *112*, 3356–3342; d) H. Miura, K. Wada, S. Hosokawa, M. Sai, T. Kondo, M. Inoue, *Chem. Commun.* **2009**, 4112–4114.
- [24] a) R. Tannenbaum, *Chem. Mater.* **1994**, *6*, 550–555; b) R. Tannenbaum, *J. Mol. Catal. A* **1996**, *107*, 207–215.
- [25] a) T. Sato, W. Mori, C. N. Kato, T. Ohmura, T. Sato, K. Yokoyama, S. Takamizawa, S. Naito, *Chem. Lett.* **2003**, *32*, 854–855; b) T. Sato, W. Mori, C. N. Kato, E. Yanaoka, T. Kuribayashi, R. Ohtera, Y. Shiraishi, *J. Catal.* **2005**, *232*, 186–198.

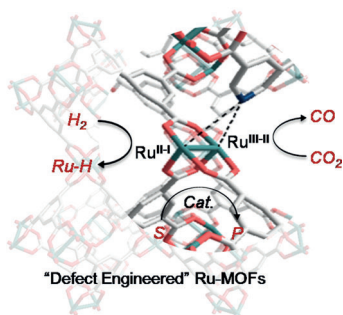
## Communications



### Metal–Organic Frameworks

O. Kozachuk, I. Luz,  
F. X. Llabrés i Xamena, H. Noei,  
M. Kauer, H. B. Albada, E. D. Bloch,  
B. Marler, Y. Wang,\* M. Muhler,  
R. A. Fischer\* ————— ■■■■—■■■■

Multifunctional, Defect-Engineered  
Metal–Organic Frameworks with  
Ruthenium Centers: Sorption and  
Catalytic Properties



The defect engineering in Ru-based metal–organic frameworks (MOFs) at coordinatively unsaturated metal centers (CUS) induces partial reduction of the metal nodes and leads to properties that are absent for the parent MOF, such as dissociative chemisorption of CO<sub>2</sub> and enhanced sorption capacity of CO. The modified MOFs offer new perspectives as multifunctional materials whose performance is controlled by design of the defects.